Journal of Crystal Growth 311 (2009) 4034–4043

Contents lists available at ScienceDirect

Journal of Crystal Growth

journal homepage: www.elsevier.com/locate/jcrysgro

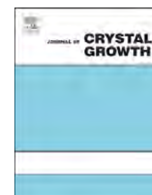

Study of the nucleation and growth of TiO_2 and ZnO thin films by means of molecular dynamics simulations

Neyda Baguer [a], Violeta Georgieva [a,*], Lazaro Calderin [b], Ilian T. Todorov [c], Sake Van Gils [d,e], Annemie Bogaerts [a]

[a] Research group PLASMANT, Department of Chemistry, University of Antwerp (UA), Universiteitsplein 1, Antwerp B-2610, Belgium
[b] Department of Physics, Queen's University, Kingston, Ontario, Canada K7L 3N6
[c] STFC Daresbury Laboratory, Daresbury, Warrington, WA4 4AD, United Kingdom
[d] OCAS, Arcelor Research Industry Ghent, Surface Functionalisation, John Kennedylaan 3, B-9060 Zelzate, Belgium
[e] FLAMAC (Flanders Materials Centre), Technologiepark 903, B-9052 Zwijnaarde, Belgium

ARTICLE INFO

Article history:
Received 23 March 2009
Received in revised form
8 June 2009
Accepted 16 June 2009
Communicated by Y. Furukawa
Available online 23 June 2009

PACS:
68.55.A–
31.15.xv
81.15.Aa

Keywords:
A1. Computer simulation
A1. Nucleation
A1 Growth models
B1. Titanium compounds (TiO_2)
B1. Zinc compounds (ZnO)

ABSTRACT

The nucleation and growth of titanium dioxide (TiO_2) and zinc oxide (ZnO) thin films on Fe_2O_3 (hematite), Al_2O_3 (α-alumina) and SiO_2 (α-quartz) are studied by molecular dynamics simulations. The results show the formation of a strong interface region between the substrate and the film in the six systems studied here. A combination of polycrystalline and amorphous phases are observed in the TiO_2 films grown on the three substrates. ZnO deposition on the Fe_2O_3 and Al_2O_3 crystals yields a monocrystalline film growth. The ZnO film deposited on the SiO_2 crystal exhibits less crystallinity. The simulation results are compared with experimental results available in the literature.
© 2009 Elsevier B.V. All rights reserved.

1. Introduction

Metal oxide thin films are gaining more and more interest due to their optical, chemical and electrical properties. Representative examples of these include titanium dioxide (TiO_2) and zinc oxide (ZnO) films, which are widely used in industrial applications.

TiO_2 films have a high refractive index and high dielectric constant; they are transparent in the visible and near-infrared range, chemically stable and non-toxic [1]. Therefore, they can be used as a pigment [2] and ultraviolet (UV) filter in the cosmetic industry, as an antireflective coating [3] in the glass industry and as a dielectric material for integrated circuits [4]. TiO_2 films also find application in the production of solar cells [5] as well as in catalysis and photocatalysis [6] like, for example, in the destruction of organic materials [7,8].

ZnO films exhibit semiconducting and piezoelectric properties, excellent ultraviolet photosensitivity and are optically transparent. These properties make them useful for the construction of thin film transistors [9,10], light emitting diodes (LED) [11,12], transparent conductive materials [13,14] and UV detectors [15,16]. Moreover, they could have novel applications in biomedical sciences because they are biosafe and biocompatible [17].

TiO_2 and ZnO films can be prepared by different techniques depending on the desired structural and mechanical properties of the coating, e.g. sputtering [18–20], evaporation [21], atomic layer deposition [22], molecular beam epitaxy [23–25], chemical vapour deposition [7,8,26–40] and pulsed laser deposition [41–43]. A number of papers investigated experimentally TiO_2 and ZnO thin films obtained by metalorganic chemical vapour deposition (MOCVD) [30–40], which is a successful technique permitting good control of deposition parameters and, consequently, of composition, microstructure and morphology of the

* Corresponding author. Fax: +32 3 265 23 76.
E-mail addresses: violeta.georgieva@ua.ac.be (V. Georgieva), annemie.bogaerts@ua.ac.be (A. Bogaerts).

0022-0248/$ - see front matter © 2009 Elsevier B.V. All rights reserved.
doi:10.1016/j.jcrysgro.2009.06.034

film. In contrast to the relatively large amount of experimental work, and even when they can provide unique insights into the growth mechanisms and structure of thin film depositions, atomistic studies of TiO_2 and ZnO films by computer simulations are scarce because of the reasons we discuss below.

Atomistic simulation techniques use either a classical mechanical approach, i.e. classical molecular dynamics (MD) and Monte Carlo (MC) methods [44] or a quantum mechanical approach, i.e. density functional theory (DFT) [45]. The DFT techniques are computationally very demanding and therefore limited to a rather small number of atoms and consequently are limited to the very initial or final stages of the film formation. For example, using periodic plane wave DFT calculations, the structure of ZnO thin film slabs terminated in different surfaces were generated (not deposited) to determine the lowest energetic configuration of the arrangement of atoms on the surfaces [46]. Another work investigates the deposition of ZnO molecules on sapphire and the temperature influence upon the surface and interface structure by DFT simulations [47]. However, DFT techniques are not yet suitable to study the mechanisms of the thin film growth. Classical MD simulations are well suited to overcome the limitations of DFT and other ab-initio techniques. However, their applications are limited by the ability to obtain high quality transferable interatomic potentials. It should also be mentioned that even the MD simulations are very CPU time consuming at the current computational power available and therefore it is rarely possible to investigate the processes in its real time. The simulated time with MD is limited to nanoseconds or less because of the small time step (in the order of fs) required for resolving the atomic vibrations. These restrictions explain the limited number of papers investigating the deposition not only of TiO_2 and ZnO films but also of other oxide films by MD simulations [48–50]. In the work of Sayle et al. [48] the authors employed three MD simulation methodologies to investigate the nucleation, growth and structure of oxides deposited on oxide substrates, showing that the substrate influences critically the structure of the deposited film, as well as the interfacial ion densities and various epitaxial relationships. Hasnaoui et al. [49] investigated the oxidation of aluminium single crystal using MD with dynamic charge transfer between atoms. An amorphous structure of the oxide film and a layer by layer growth mode were observed. Finally, Taguchi and Hamaguchi [50] studied the SiO_2 deposition process by MD combined with MC simulations emulating thermal relaxation between two successive depositions.

The present work investigates the nucleation and growth of thin TiO_2 and ZnO films on Al_2O_3 (α-alumina), Fe_2O_3 (hematite) and SiO_2 (α-quartz) by MD simulations. The influence of the different substrates on the film structure is discussed. The simulation results are compared with experimental results, available in the literature for TiO_2 and ZnO films deposited by MOCVD.

2. Description of the model

The deposition process of TiO_2 and ZnO molecules on Fe_2O_3, Al_2O_3 and SiO_2 is simulated using the MD package, DL_POLY_3 [51]. A driving program was written to automate the deposition of molecules on the surface and relaxation of the system. In the MD method the trajectory of all particles is generated by solving the Newton equation of motion

$$\vec{r} = \vec{r}_0 + \vec{v}_0 \Delta t + \frac{\vec{F}}{2m}\Delta t^2, \vec{F} = -\vec{\nabla} V \tag{1}$$

where $\vec{r}_0, \vec{v}_0$ are the initial position and velocity for a given particle, $\vec{F}$ the total force acting on the particle and Δt the time step. The force is assumed to be conservative, and therefore, can be expressed as a gradient of the interatomic potential, V. Hence, the interatomic potential becomes the basic input for the simulation, and its quality is the major factor in determining the reliability of the results. In practice, finding a classical potential that describes all the interatomic interactions only on theoretical basis is a paramount task. Therefore, it is necessary to introduce some assumptions to simplify the many-body interaction problem. One way of doing that is by calculating the potential energy on the base of empirical considerations. Potential parameters can also be obtained semi-empirically using both experimental and theoretical data, or by fitting parameters to potential curves calculated theoretically.

In this work, the interactions between the atoms are described by an ionic potential [52]. The potential energy is assumed additive and the interactions are divided into long-range and short-range interactions. At long range the potential energy of the system is a purely electrostatic Coulomb interaction between two ionic point charges. At short range a potential energy $V_{short\text{-}range}$, due to the repulsion between electron clouds, is considered as a balancing counterpart to the Coulomb potential. The total potential is given by

$$V = \frac{1}{4\pi\varepsilon_0}\sum_{ij}\frac{q_1 q_2}{r_{ij}} + V_{short-range} \tag{2}$$

where q_1 and q_2 are the ionic charges, r_{ij}, the distance between the ith and jth ions, and ε_0 the vacuum permittivity. For the short-range potential, different analytical expressions are proposed in the literature. Here, the short-range interactions are described by the two-body empirical Buckingham potential [53]

$$V_{Buckingham} = A\exp\left(-\frac{r_{ij}}{\rho}\right) - \frac{C}{r_{ij}^6} \tag{3}$$

where the parameters A, ρ, C are particular to each pair cation–anion and anion–anion interactions. The cation–cation interactions are considered to be only of electrostatic type [53]. The exponential part of the Buckingham potential describes the repulsion between the shells of bound electrons due to Pauli's exclusion principle. The negative power term describes an induced dipole attraction or Van der Waals interaction, which is present due to any asymmetry in the electron density distribution. A three-body term is added to the Buckingham potential to better represent short range interactions in SiO_2 as discussed below.

Note that the Zn–O bond has also a covalent besides an ionic character. However, Zn belongs to a d-block metal group 12 and its compounds do not involve in the ionization of d shell [54]. In this sense, Zn behaves more like an alkali metal. Coulomb plus Buckingham potentials are known to work well for alkali and alkaline earth metal compounds [55,56]. Therefore, we have chosen these potentials to describe the interactions for ZnO as well.

In general the potentials have limited applicability for describing the surface interactions with the same parameters, which were calculated by fitting to the bulk properties. Therefore, the simulation of deposition depends strongly on the potential, which is used. We tested 4 potential sets for TiO_2 and choose the one that gave best agreement with experimentally deposited films. Using the other 3 potential sets either made the simulation unstable or the simulation yielded a porous film. The difference between the outputs of the 4 sets can be a consequence of their fitting procedure. First, the partial charge model proposed by Matsui and Akaogi [57] was applied. It was observed that the calculations become very unstable when Ti and O ions come very close to each other. Therefore, this approach was not successful and subsequently the interactions in TiO_2 were treated by the

formal charge models [58–60]. In Ref. [58], the potential parameters were obtained by least square fitting to the lattice parameters and assumed to be transferable between all three TiO_2 polymorphs, since no angular dependence is accounted for in the Buckingham function and the interatomic distances between the O^{2-}–O^{2-} and Ti^{4+}–O^{2-} are very similar in all the TiO_2 polymorphs. In Ref. [59], the potential parameters were fitted to the anatase lattice constants, using the so called "relaxed" least square fitting. However, these two potentials [58,59] yielded a porous film. Finally, the potential parameters obtained semi-empirically [60], i.e. they were fitted to a potential, which was calculated based on the modified electron gas theory [61], yields a film in agreement with the experiments. We considered this potential set as the most reliable for deposition of the TiO_2 films.

For ZnO, the first potential set [62] we have tested, showed that the simulated ZnO film growth is in close agreement with the experiment, which means that the used potential describes the surface interactions in a reasonable way. The potential parameters in this set were obtained by fitting to the crystal structure and properties of ZnO, calculated using classical and quantum mechanical methods.

The Buckingham potential parameters for the cation–anion and anion–anion interactions in Fe_2O_3 from Refs. [53,63], and in Al_2O_3 from Ref. [64], and full charge model were used in the present simulation. The O^{2-}–O^{2-} Buckingham potential parameters were derived semi-empirically by Catlow et al. from the free-ion Hartree–Fock self-consistent field method [63]. In Refs. [53,63] the potential parameters were obtained by least square fitting to experimental lattice parameters, and dielectric and elastic constants.

The potentials so far described contain only two-body functions and are well suited for describing ionic bonds. However in the case of SiO_2, along with the significant ionic bond, it has a strong, directional covalent bond. Two potential forms are mainly found to describe this kind of interactions in the literature. The first potential form considers only two-body interactions and the Coulomb interactions are weakened by using partial charges. The second potential form is a sum of Coulomb potential with full ionic charges, and the short-range potential, which is the sum of a two-body term in Buckingham form and a three-body term to include the directional dependency of the bonding. We have investigated both types of potentials. The first potential, which considers partial electrostatic charges coupled with a Morse potential for the short-range interactions, was tested by the potential sets developed by Demiralp [65] and Takada [66]. We found these potential sets not suitable for the simulation of deposition because the system becomes unstable when deposition started. The second potential form was tested by two potential sets presented by Malavasi et al. [67], where the Buckingham parameters are the same for the two sets. The authors proposed the three-body screened Vessal potential [68] or the three-body truncated Vessal potential [68,69]. Both Vessal potentials worked well. However, they slowed down the computational time substantially, especially when the three-body potential in the form of truncated Vessal function is used. Therefore, we considered the screened Vessal potential to simulate the three-body interaction in the SiO_2 substrate and the potential parameters for Buckingham and three-body term have been taken from Ref. [67]. In the screened Vessal function [68] the three-body interactions in the Si–O–Si and O–Si–O triads are described by

$$V_{ves1}(r_{ij}, r_{ik}, \vartheta_{jik}) = \frac{k}{8(\vartheta_{jik}-\pi)^2}[(\vartheta_0-\pi)^2 - (\vartheta_{jik}-\pi)^2]^2 \exp\left[-\left(\frac{r_{ij}+r_{ik}}{\rho}\right)\right] \quad (4)$$

where ϑ_0 is the equilibrium bond angle, k the three-body spring constant and ρ the spherical cutoff, given as a specific distance from the central atom. The cutoff is selected to increase the order around Si as a centre and to decrease the order around O, i.e. the connecting bond in the tetrahedrons. In general, the three-body contribution accounts for less than 0.1% of the total potential energy, but it is important for the stiffness of the $Si–O_4$ tetrahedron [70].

The data for the crystal structures of Fe_2O_3, Al_2O_3 and SiO_2 were taken from the database MINCRYST [71]. Fe_2O_3 and Al_2O_3 both have a corundum-type crystal structure and space group R3c. The primitive unit cell of the corundum crystal is rhombohedral. However, in the present context, it is more convenient to describe it by the hexagonal non-primitive unit cell, which contains 30 atoms. Each Al or Fe atom in this crystal is coordinated to six O atoms and each O atom to four Al or Fe atoms. For the SiO_2, we have selected the α-crystal structure, which has a hexagonal primitive unit cell with 9 atoms and space group $P32_1$. In α-quartz, each Si atom is bound to four O atoms in a $Si–O_4$ tetrahedral coordination, while each O atom is bound to two Si atoms which link the tetrahedrons in a continuous network.

The MD calculations were carried out in a simulation box with three-dimensional (3D) periodic boundary conditions. The surface (0001) was emulated by adding vacuum gaps in z-direction above and below the substrate. The substrate slab was separated from its nearest periodic image by a vacuum gap of 20 Å to avoid self-interaction. The simulation box was symmetrical in the direction-xy plane as depositing molecules were placed both above and below the substrate to prevent the generation of instantaneous dipole moment. The 3D periodicity was required for the calculation of the Coulomb potential through the Ewald summation technique [72], which is computationally efficient and unconditionally convergent. The dimensions of the simulated box were obtained by scaling the corresponding unit cell so that the length in each direction is at least two times greater than the cutoff radius for the long-range interactions, which is set to 9 Å in the present study. The initial substrates consist of 5000–6000 atoms and the dimensions are in the order $(40 \times 40 \times 30)$ Å. All substrate atoms are allowed to move.

The initial (x,y,z) coordinates of each molecule (TiO_2 or ZnO) to be deposited were randomly sampled at a distance between 8 and 11 Å above the (0 0 0 1) substrate surface. The initial velocity of the molecules was calculated for an energy of 0.066 or 0.075 eV, which corresponds to the substrate temperature of 770 K (in case of deposition on the Si_2O substrate) or 870 K (in cases of deposition on the Al_2O_3 and Fe_2O_3 substrates), with a direction perpendicular to the surface of the substrate. The initial bond length and O–Ti–O bond angle were set to 3.8 Å and 117.9° according to the study of the ground-state geometry of TiO_2 molecules [73]. The initial bond length in the ZnO molecule was set to 1.98 Å based on the Zn–O bond length in the ZnO crystal. The time step was chosen to be variable and is calculated in the model in the order of 1–2 fs. The variable time-step algorithm was used to shorten the time to solution of the simulations and to ensure satisfactory numerical stability of the integration algorithms. This is necessary when the dynamics of the system changes its pace considerably, usually due to the nature of the virtual experiment. A fixed time stepping can make the simulation (i) numerically unstable when the time step is too big and (ii) computationally too expensive if the time step is too short. The variable time-step algorithm adjusts the time-step value so that the integration is in the most favourable regime: the shortest time to obtain a solution without compromised numerical accuracy [51]. For example, when the deposition of a molecule is simulated the time step is usually shortened (approaching 0.5 fs) because the deposited atoms move faster than the substrate atoms. Once the

depositing molecule reaches the surface the time-step self-adjusts to about 2 fs.

The deposition of each molecule was simulated for ~15,000 time steps, i.e. ~15–30 ps, with the *NVE*-ensemble (i.e. the number of particles *N*, system volume *V* and total energy *E* are kept constant). After the deposition the system was relaxed to constant temperature of 770 K (in case of deposition on the Si_2O substrate) or 870 K (in cases of deposition on the Al_2O_3 and Fe_2O_3 substrates), which is the substrate temperature, for ~20,000 time steps, i.e. ~40 ps, with the *NVT* ensemble (i.e. the number of particles *N*, system volume *V* and temperature *T* are kept constant). In each simulation in the order of 1000 TiO_2 molecules or 500 ZnO molecules were deposited on each surface so that the films grow to at least 3 nm and the total deposition time reaches the order of 10–50 ns.

3. Results

3.1. Analysis of the growth of thin TiO_2 films on Fe_2O_3, Al_2O_3, and SiO_2

3.1.1. Initial stage of the TiO_2 film formation

Figs. 1 and 2 show snapshots of the initial stages of the growth of TiO_2 films on the Fe_2O_3 and SiO_2 substrates, respectively. The nucleation mechanism of the TiO_2 film on the Al_2O_3 substrate was found to be similar to the case of the Fe_2O_3 substrate presented in Fig. 1 and therefore is not shown here. During the formation of the first monolayer, the deposition of TiO_2 molecules (Figs. 1(a) and 2(a)) resembled a non-dissociative adsorption (the molecules did not dissociate when deposited on the substrate). The Ti ion bound preferentially with the O ions of the crystal, while the O ion of the TiO_2 molecules bound with the Fe (Al, Si) ions of the lattice. When the first TiO_2 molecules were adsorbed on the SiO_2 substrate, and a new TiO_2 molecule impinged onto a place where adsorbate atoms were already present in the neighborhood, the new TiO_2 molecule tended to bind through the Ti–O bonds with another TiO_2 molecule, rather than to the substrate atoms, which is the preferred binding mechanism for the Fe_2O_3 and Al_2O_3 substrates. In Figs. 1(b) and 2(b) one can see that at the early stage of the film formation, regions of quasi-ordered arrangement of Ti and O atoms were present. It was also observed that some Ti ions bound to the substrate O ions, which had already migrated to the film as a result of the surface reconstruction.

3.1.2. Further growth of thin TiO_2 films

Fig. 3 (a)–(c) present snapshots of the deposited TiO_2 films on the Fe_2O_3, Al_2O_3, and SiO_2 substrates, respectively. It was observed that the TiO_2 film grew on the three substrates by islands and its structure was a mixture of amorphous and polycrystalline phases.

The calculated Ti–O and O–O radial distribution functions (RDFs) of the TiO_2 films deposited on the Fe_2O_3, Al_2O_3 and SiO_2 substrates are plotted in Fig. 4(a) and (b), respectively. The corresponding RDFs in the TiO_2 crystalline rutile and anatase phases are also shown. Comparison of the RDFs in the films to the corresponding ones in the crystalline phases makes it difficult to conclude which crystalline phase was observed in the films due to significant presence of amorphous structure in the films. In addition, the crystalline regions are not large enough to be distinguished from the amorphous regions to be analyzed separately. Moreover, the randomly orientated small crystals result in a RDF close to the RDF describing an amorphous structure, for which the profile typically consists of one peak at the bond length between the two atoms and further it has values close to 1. Therefore, the angular distribution function (ADF) of the O–Ti–O bond angle was also calculated. Both RDFs and ADFs were calculated at the end of the simulation when the snapshots were taken. The ADFs of the three investigated films are presented in Fig. 5 and compared with the O–Ti–O ADFs in the rutile and anatase crystalline phases. The ADF of the TiO_2 film deposited on the Al_2O_3 substrate shows a broad maximum which covers the broad maximum in rutile at 90° and a second maximum at 165°, which is close to the second maximum in the rutile crystal at 175° Hence, the crystalline regions that are observed in the TiO_2 film deposited on the Al_2O_3 (see Fig. 3(b)) can probably be described as rutile. The ADF of the TiO_2 film deposited on the Fe_2O_3 substrate shows one broad maximum that covers the maximum in rutile at 90° while the maximum in the ADF of the film deposited on SiO_2 is moved to 100° where a broad maximum in anatase is found. Therefore, the films deposited on the Al_2O_3 and Fe_2O_3 substrate have a structure, which could be described as randomly oriented rutile crystals embedded in the amorphous structure, while the film deposited on the SiO_2 substrate is more amorphous like.

The calculated coordination number of the Ti atom in the films supports this conclusion. The Ti coordination number was defined when the O–Ti–O ADF was calculated, more specifically by counting the number of the nearest neighbor O atoms at a distance where the first maximum in the Ti–O RDF was found, i.e. 1.7–2.2 Å. If the film has a crystalline structure then the coordination number is close to the coordination number

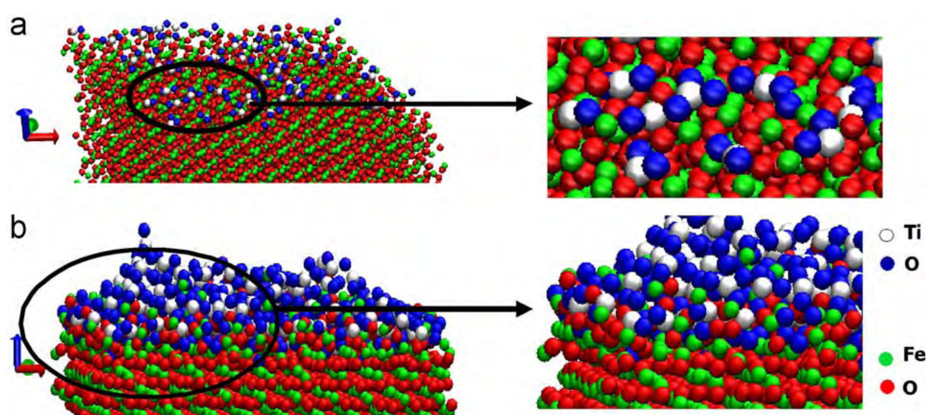

Fig. 1. Formation of the first monolayer (a) and further growth (b) of a TiO2 film on a Fe2O3 (hematite) substrate. The color scheme is shown in the figure. In all presented figures the color scheme of the axes is as follows: *x*-axis is red, *y*-axis is green and *z*-axis is blue. (For interpretation of the references to colour in this figure legend, the reader is referred to the web version of this article.)

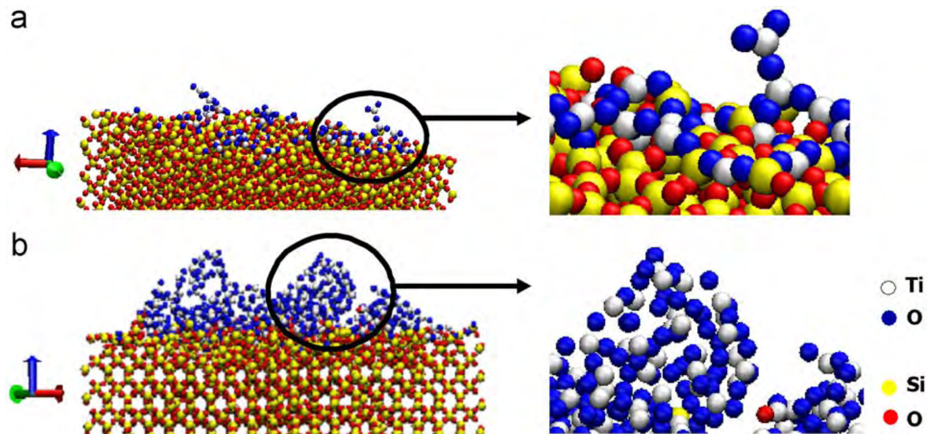

Fig. 2. Formation of the first monolayer (a) and further growth (b) of a TiO2 film on a SiO2 (α-quartz) substrate. The color scheme is shown in the figure. (For interpretation of the references to colour in this figure legend, the reader is referred to the web version of this article.)

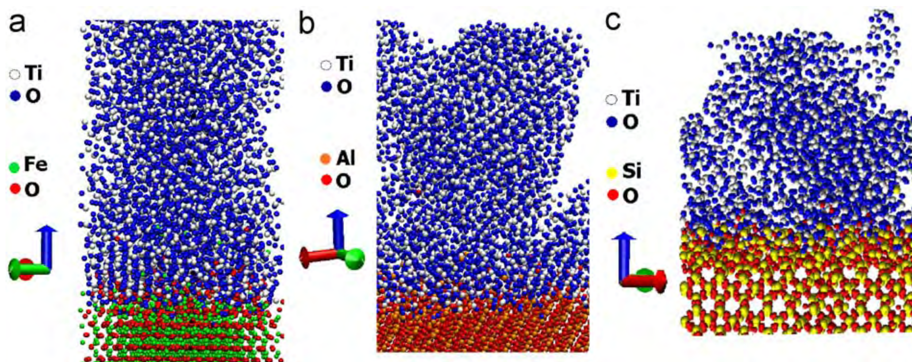

Fig. 3. Axial views (along the *z*-axis) of the TiO2 film growth on the Fe2O3 (a), Al2O3 (b) and SiO2 (c) substrates. The color scheme is shown in the figure. (For interpretation of the references to colour in this figure legend, the reader is referred to the web version of this article.)

calculated in a perfect crystal. If the film has an amorphous structure, the coordination number will decrease based on the simple reasoning for close packing in the crystal. The coordination number of Ti in perfect rutile and anatase structures is 6, while the coordination number of Ti in the films deposited on the Fe_2O_3, Al_2O_3 and SiO_2 substrates are calculated to be 5.1, 5.4 and 4.4, respectively.

Experimentally, it was found that TiO_2 films growing on steel by MOCVD at atmospheric pressure and temperature in the range 500–700 °C had a polycrystalline structure, which was a mixture of anatase and rutile phases [35] whereas on alumina only rutile phase was observed [32]. XRD measurements found that randomly oriented polycrystalline anatase structures were observed in TiO_2 films deposited on quartz by CVD [36].

3.2. Analysis of the growth of ZnO films on Fe_2O_3, Al_2O_3 and SiO_2

3.2.1. Initial stage of the ZnO film formation

Figs. 6 and 7 present snapshots of the initial stages of the growth of ZnO films on the Fe_2O_3 and SiO_2 substrates, respectively. The nucleation mechanism of the ZnO film on the Al_2O_3 substrate was similar to that on the Fe_2O_3 substrate presented in Fig. 6 and, therefore, is not shown here. Similar to the case of TiO_2 film formation, when ZnO molecules were deposited on the Fe_2O_3, Al_2O_3, or SiO_2 substrates, the ZnO molecules did not dissociate immediately either. During the formation of the first monolayer, the O ion of the ZnO adsorbate bounds to the cation of the crystal whereas the Zn bound to the O ions of the substrate. In the vicinity of both types of molecules (substrate and adsorbate) the next impacting ZnO molecules tended to bind to the already deposited ZnO forming some chains of successively bonded ZnO molecules. It is worth noticing that already during the formation of the first monolayer of ZnO on the Fe_2O_3 (and Al_2O_3) substrate, the O and Zn ions tended to lie parallel to each other and to the Fe and O ions of the substrate, which was not observed in the growth mechanism on the SiO_2 substrate (compare Figs. 6(b) and 7(b)).

3.2.2. Further growth of the thin ZnO film

Snapshots of the simulated ZnO films on the Fe_2O_3, Al_2O_3 and SiO_2, substrates, are shown in Fig. 8(a–c), respectively. During the formation of the next monolayers, following the first monolayer in the films deposited on the Fe_2O_3 and Al_2O_3 substrates, the alignment of Zn and O atoms was observed almost over the entire layer (Figs. 8(a) and (b)), while in the film deposited on the SiO_2 substrate only small regions of ordered structure were observed (Fig. 8(c)). The pattern of the ZnO film growth on the Fe_2O_3, Al_2O_3 and SiO_2 substrates differed from the one obtained

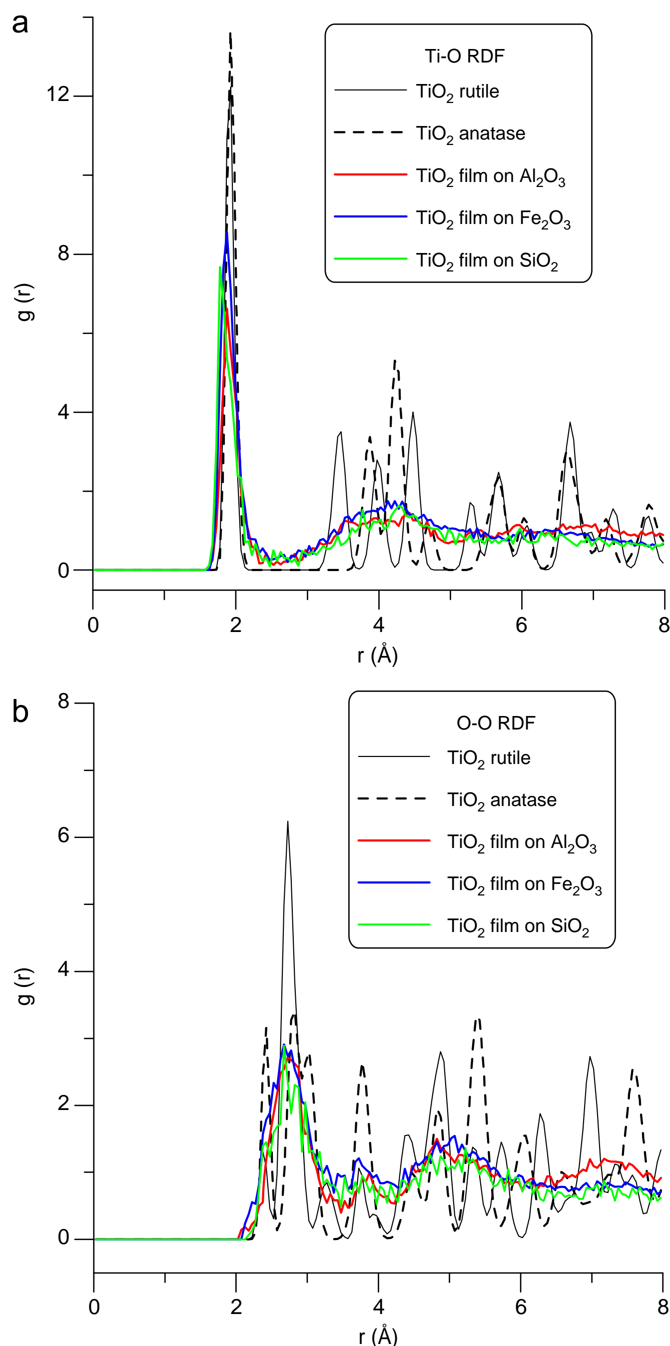

Fig. 4. Calculated Ti–O (a) and O–O (b) RDFs of the deposited TiO2 films on the Fe2O3, Al2O3 and SiO2 substrates. The corresponding RDFs of relaxed TiO2 rutile and anatase crystals are also shown for comparison.

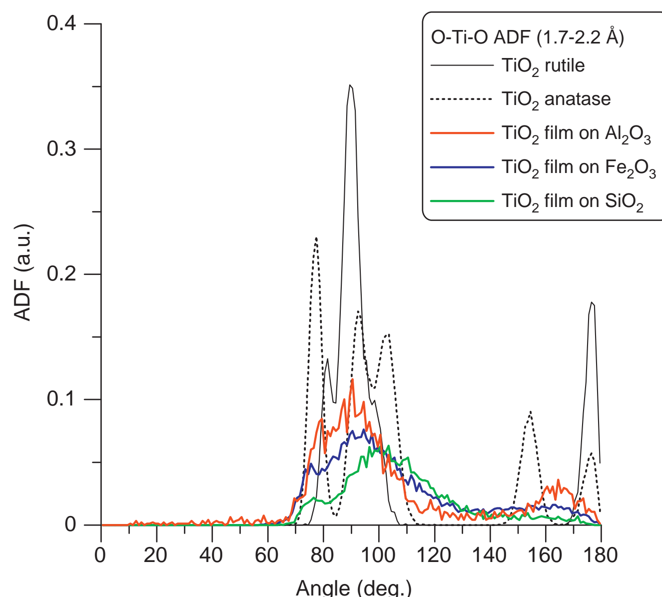

Fig. 5. Calculated O–Ti–O bond ADFs of the deposited TiO2 films on the Fe2O3, Al2O3 and SiO2 substrates. The corresponding ADFs in relaxed TiO2 rutile and anatase crystals are also shown for comparison.

for the TiO_2 film. In general, the deposition of ZnO molecules produced a better coverage for the three substrates, as well as a more uniform mass distribution and a higher average density, compared to that of the TiO_2 molecules on the same substrates and at the same simulation parameters. The ZnO films deposited on the Fe_2O_3 and Al_2O_3 substrates showed an epitaxial growth with good crystallinity (Figs. 8(a) and (b)). Epitaxial growth of thin ZnO films growing on Al_2O_3 substrates at atmospheric pressure by MOCVD has also been reported by several authors for similar conditions [37,38]. The simulated film grew with the main crystallographic *c*-axis parallel to the (0001) Al_2O_3 substrate, which was also observed by the films deposited by MOCVD at temperature of 773 K [39,40]. The prevalence of *c*-axis oriented ZnO films has also been observed by other deposition techniques [41–43].

In the case of ZnO deposition on SiO_2 (see Fig. 8(c)), the film showed crystalline regions, but it was not a monocrystalline structure as in the case of ZnO films on the Fe_2O_3 and Al_2O_3 substrates (compare with Figs. 8(a) and (b)). The corresponding Zn–O and O–O RDFs are presented in Fig. 9(a) and (b) and are compared with the Zn–O and O–O RDFs calculated in the perfect ZnO crystal. The interatomic distances between the Zn–O and O–O atoms of the ZnO films are similar for the three substrates as seen from the RDF's. The O–Zn–O bond ADFs was also calculated. Fig. 10 compares the O–Zn–O ADFs in the three deposited films with the ADF in a relaxed ZnO crystal and reasonable agreement is observed. The ADFs of the three films show a broad maximum at 115°, which is very close to the broad maxima at 110° in the ZnO relaxed crystal structure. The second maximum observed in the ADF of the film deposited on the Al_2O_3 substrates at 90° could be due to the atoms occupying the sites in the film-substrate interface and/or the sites in the free surface.

The comparison of the calculated coordination number of Zn in the ZnO films deposited on the Fe_2O_3, Al_2O_3 and SiO_2 substrates (3.6, 3.6 and 3.2, respectively) with the coordination number of Zn in the ZnO perfect crystal (i.e. 4) also confirms that the crystallinity in the film deposited on the SiO_2 substrate is lower. The Zn coordination number was defined when the O–Zn–O ADF was calculated, more specifically by counting the number of the nearest neighbor O atoms at a distance where the first maximum in the Zn–O RDF was found, i.e. 1.5–2.5 Å.

4. Discussion

The simulated growth of TiO_2 or ZnO films on the Fe_2O_3 and Al_2O_3 substrates developed in a similar manner on both substrates as the TiO_2 films grew as an amorphous structure combined with polycrystals whereas the ZnO film grew more as a monocrystal. The similarity of growth behaviour on the two substrates could be

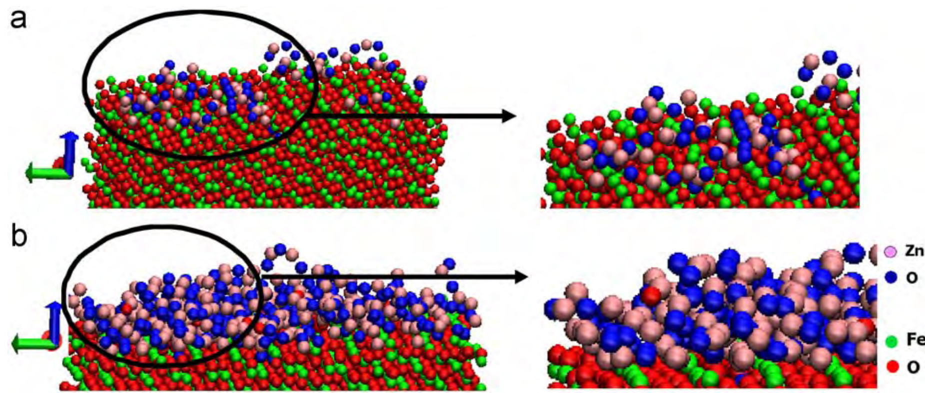

Fig. 6. Formation of the first monolayer (a) and further growth (b) of a ZnO film on a Fe2O3 (hematite) substrate. The color scheme is shown in the figure. (For interpretation of the references to colour in this figure legend, the reader is referred to the web version of this article.)

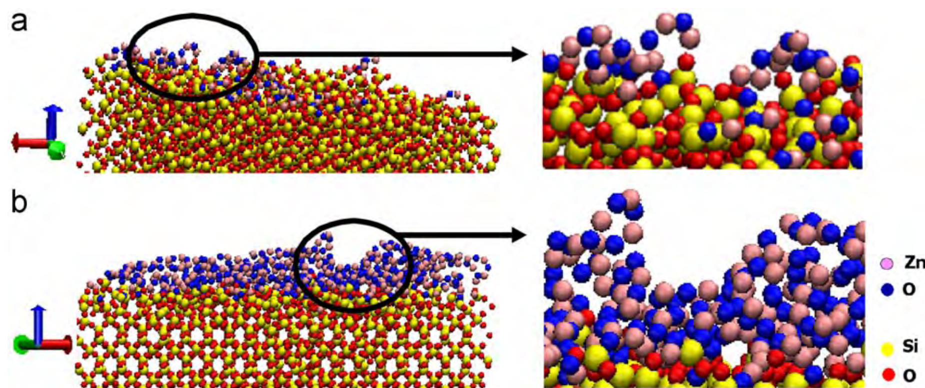

Fig. 7. Formation of the first monolayer (a) and further growth (b) of a ZnO film on a SiO2 (α-quartz) substrate. The color scheme is shown in the Figure.

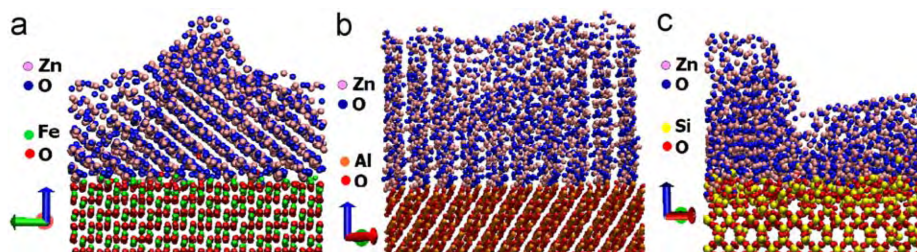

Fig. 8. Axial views (along the *z*-axis) of the ZnO film growing on the Fe2O3 (a), Al2O3 (b) and SiO2 (c) substrates. The color scheme is shown in the figure. (For interpretation of the references to colour in this figure legend, the reader is referred to the web version of this article.)

due to both crystals having the same structure (corundum), similar cohesive energies and constituent cations and anions with the same formal charges.

There are a few arguments to reason why the ZnO films would grow as a monocrystal on the Fe_2O_3 and Al_2O_3 substrates while the TiO_2 would form polycrystal films. First, ZnO (zincite), Al_2O_3 (α-alumina) and Fe_2O_3 (hematite) crystals have hexagonal unit cells, which facilitate the epitaxial growth, while TiO_2 rutile and TiO_2 anatase have tetragonal unit cells. Second, Zn behaves, in some ways, as an alkali metal although it belongs to the d-block metals while Ti is a transition metal (see above), and it is known that alkali metals generally give rise to films with good crystallinity [1]. Finally, it is known that a good deposition on the surface occurs, when the interaction energy between the depositing atoms is weaker than the interaction energy between them and the atoms of the substrate surface. The main contribution to the total configurational energy, in the case of an ionic system, is due to the Coulomb potential energy. Indeed, the short-range potential energy represents on average, around 10% of the total configurational energy of the system. The Ti–O and Zn–O Coulomb, Buckingham, and total (Coulomb+Buckingham) potential energy, calculated with the potential parameters used in the present simulation, is shown as a function of the distance between the ions in Fig. 11. It is observed that at a distance of 1.9–2.0 Å, which corresponds to the bond lengths in Ti–O and Zn–O in the films and corresponding crystals the Coulomb part of the total potential energy is dominant (see Fig. 11(b)). Hence, one explanation for the better coverage of ZnO films compared to TiO_2 films can be based

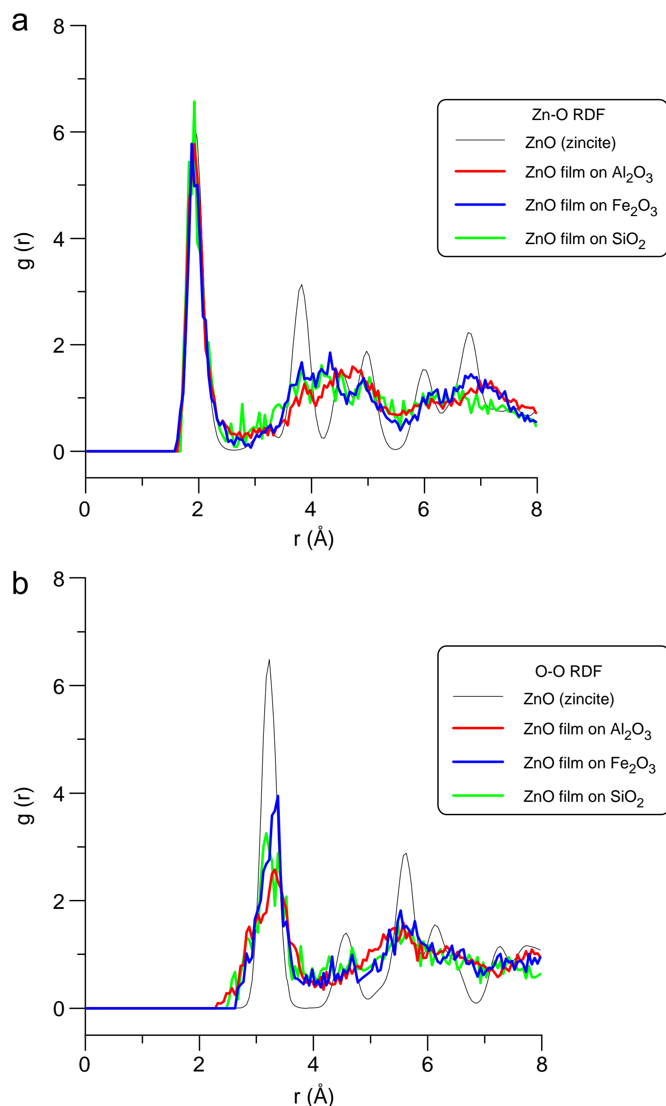

Fig. 9. Calculated Ti–O (a) and O–O (b) RDFs of the deposited ZnO films on the Fe2O3, Al2O3, and SiO2 substrates compared with the corresponding RDFs of a relaxed ZnO (zincite) crystal.

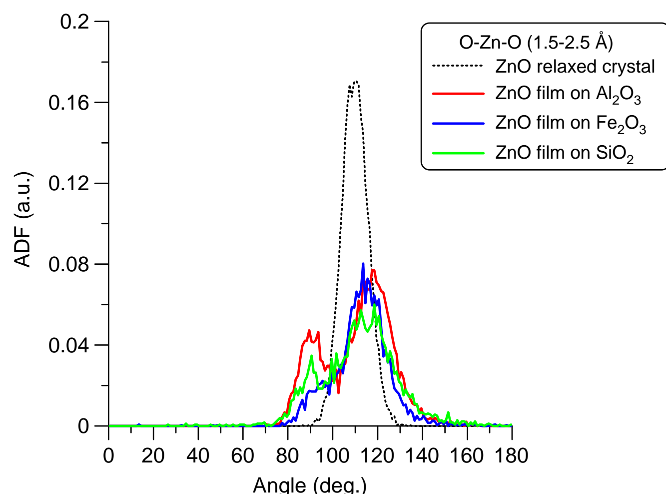

Fig. 10. Calculated O–Zn–O bond ADFs of the deposited ZnO films on the Fe2O3, Al2O3 and SiO2 substrates. The corresponding ADF in a relaxed ZnO crystal is shown for comparison.

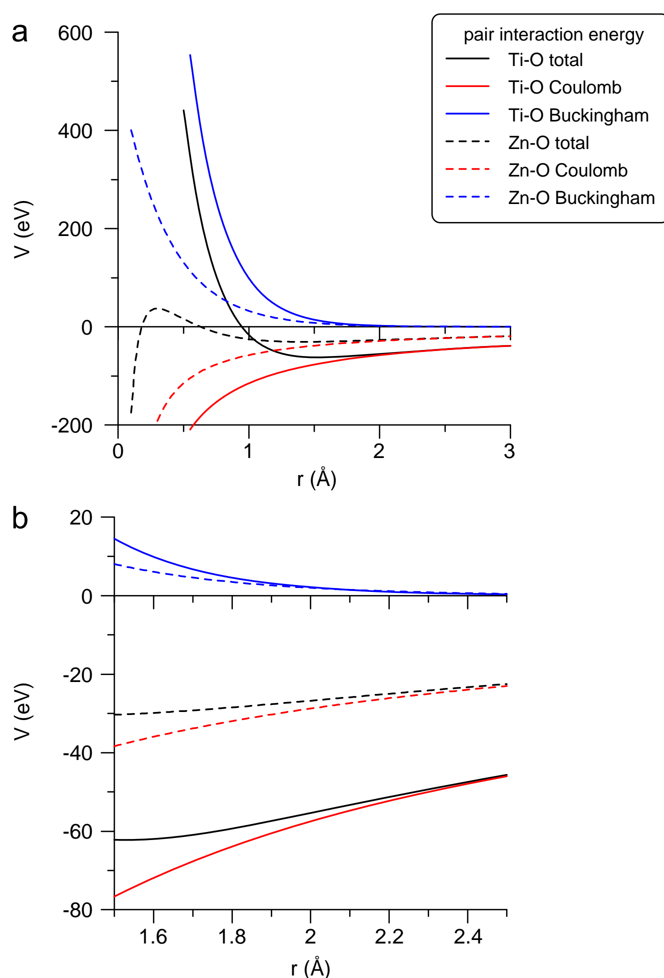

Fig. 11. Ti–O and Zn–O Coulomb, Buckingham and total (Coulomb+Buckingham) potential energy *V*(eV) as a function of distance between the ions *r*(Å) (a). The plot presented in (b) is a zoomed view of the plot presented in (a) for distances *r* between 1.5 and 2.5 Å.

on the difference of electric charges of Zn and Ti ions (Zn^{2+} interacting with O^{2-} compared to Ti^{4+} interacting with O^{2-}) which suggests a weaker interaction energy between Zn–O than between Ti–O.

Both TiO_2 and ZnO films deposited on the SiO_2 substrate exhibit a more amorphous-like structure. We think that one possible reason is the change in the structure of the upper layers of the SiO_2 substrate (see Figs. 3(c) and 8(c)). It seems that amorphization of the substrate surface affects the growing film. As it is explained in Section 2, SiO_2 has a well-defined local structure by forming a Si–O_4 tetrahedron. The O atom is bound to two Si atoms and in this way linking the tetrahedrons. This "bridge" bond between two Si atoms is flexible, i.e. the Si–O_4 tetrahedrons can be linked at widely varying angles, which results in SiO_2 having many different possible crystalline structures, and can very easily form amorphous materials. The most stable crystalline form under normal conditions is α-quartz [74]. We suppose that the deposited molecules can break the long-range order in the SiO_2 α-quartz and therefore the surface layers form an amorphous structure. In turn, this amorphous structure affects the structure of deposited film.

Finally, it is worth mentioning that although the MD simulations can provide a valuable insight into the film growth process, as it is shown above, the simulated time with MD is limited to nanoseconds or less. The reason is the time step, which has to be

small enough to resolve the atomic vibrations, i.e. in the order of femtoseconds. In the present study, the films have grown at least to 3 nm for 10–50 ns and therefore, deposition rate in the simulation is in the order of 10^9–10^{10} nm/min while typical experimental deposition rate is in the order of 1–10^2 nm/min [35]. Hence, the simulated deposition rates are several orders of magnitude higher than the experimental deposition rates. Thermally activated processes with low rates are excluded in the MD simulations. Therefore, other methods should be employed to extend the simulation time scale and, in this way, phenomena such as terrace diffusion and interlayer transport to be considered. Recently, several accelerated dynamics methods were proposed [75]. As a further improvement of our study we will consider coupling one of the accelerated dynamics methods with MD to achieve simulation deposition rates in the order of the experimental deposition rates.

5. Conclusions

The present work investigates the nucleation and growth of TiO_2 and ZnO thin films on three different substrates (Fe_2O_3, Al_2O_3 and SiO_2) by a MD simulation. The results can be summarized as follows:

In the six systems studied here, the formation of a strong interface region between the substrate and the film was observed; therefore, a good adhesion of the TiO_2 and ZnO films to the substrate can be expected.

The TiO_2 films on the three investigated substrates grew by islands. The films deposited on the Al_2O_3 and Fe_2O_3 substrate have a structure that is a mixture of amorphous and rutile phases, while the film deposited on the SiO_2 substrate has mainly an amorphous structure. The structure of the film deposited on the Al_2O_3 substrate is in good agreement with experimental observations from literature.

The ZnO films deposited on the Fe_2O_3 and Al_2O_3 substrates exhibited a monocrystalline structure, which correlates well to the structures of experimentally deposited films on an Al_2O_3 substrate. The ZnO film deposited on the SiO_2 substrate, on the other hand, showed a less crystalline structure.

Our results are in reasonable qualitative agreement with experimental observations found in literature, which confirms that such simulations can provide a realistic picture of the film growth, and can be used for a better understanding of the underlying mechanisms.

Acknowledgments

This work was supported by the Flanders Materials Center (FLAMAC) and the IWT. The authors would like to thank E. Neyts (UA), J. Paul (FLAMAC), and G. Huyberechts (Umicore) for the interesting discussions. Calculations have been performed on the CALCUA supercomputer of the University of Antwerp.

References

[1] U. Diebold, Surf. Sci. Rep. 48 (2003) 53.
[2] J. Hewitt, Cosmet. Toiletries 114 (1999) 59.
[3] K.H. Ahn, Y.B. Park, D.W. Park, Surf. Coat. Technol. 171 (2003) 198.
[4] K. Vydianathan, G. Nuesca, G. Peterson, E.T. Eisenbraun, A.E. Kaloyeros, J. Mater. Res. 16 (2001) 1838.
[5] A. Goosens, E.L. Maloney, J. Schoonman, Chem. Vapor Deposition 4 (1998) 109.
[6] I.K. Konstantinou, T.A. Albanis, Appl. Catal. B: Environ. 42 (2003) 319.
[7] A. Mills, N. Elliot, I.P. Parkin, S.A. O'Neill, R.J. Clark, J. Photochem. Photobiol. A: Chem. 151 (2002) 171.
[8] S.A. O'Neill, R.J. Clark, I.P. Parkin, N. Elliot, A. Mills, Chem. Mater. 15 (2003) 46.
[9] E.M. Fortunato, P.M. Barquinha, A.C. Pimentel, A.M. Goncalves, A.J. Maeques, L.M. Pereira, R.F. Martins, Adv. Mater. 17 (2005) 590.
[10] T. Hirao, M. Furuta, H. Furuta, T. Matsuda, T. Hiramatsu, H. Hokari, M. Yoshida, M. Ishii, M. Kakegawa, J. Soc. Inf. Dev. 15 (2007) 17.
[11] A. Tsukazaki, A. Ohtomo, T. Onuma, M. Ohtani, T. Makino, M. Sumiya, K. Ohtani, F. Shigefusa, S..F. Chichibu, S. Fuke, Y. Segawa, H. Ohno, H. Koinuma, M. Kawasaki, Nat. Mater. 4 (2005) 42.
[12] A. Tsukazaki, M. Kubota, A. Ohtomo, T. Onuma, K. Ohtani, H. Ohno, S.F. Chichibu, M. Kawasaki, Jpn. J. Appl. Phys. 44 (2005) L643.
[13] T. Minami, Semicond. Sci. Technol. 20 (2005) S35.
[14] R. Ghosh, D. Basak, S. Fuhihara, J. Appl. Phys. 96 (2004) 2027.
[15] H. Ohta, M. Hirano, Appl. Phys. Lett. 83 (2003) 1029.
[16] J. Cheng, Y. Zhang, R. Guo, J. Cryst. Growth 310 (2008) 57.
[17] J.L. Wang, Mater. Today 7 (2004) 26.
[18] J.T. Brown, Appl. Opt. 43 (2004) 4506.
[19] T. Matsuda, M. Furuta, T. Hiramatsu, C. Li, H. Furuta, H. Hokari, T. Hirao, J. Cryst. Growth 310 (2008) 31.
[20] L.S. Kim, T.H. Kim, S.S. Kim, C.R. Lee, B.T. Lee, J. Cryst. Growth 299 (2007) 295.
[21] T. Fujii, N. Sakata, J. Takada, Y. Miura, Y. Daitoh, M. Takano, J. Mater. Res. 9 (1994) 1468.
[22] A. Rathu, M. Ritala, Chem. Vapor Deposition 8 (2002) 21.
[23] N. Izyumskaya, V. Avrutin, W. Schoch, A. El-Shaer, F. Reuß, Th. Gruber, A. Waag, J. Cryst. Growth 269 (2004) 356.
[24] T. Matsumoto, H. Kato, K. Miyamoto, M. Sano, Appl. Phys. Lett. 81 (2002) 1231.
[25] A. Bakin, A. El-Shaer, A. Che Mofor, M. Kreye, A. Waag, F. Bertram, J. Christen, J. Stoimenos, J. Cryst. Growth 287 (2006) 7.
[26] S.I. Cho, C.H. Chung, S.H. Moon, Thin Solid Films 409 (2002) 98.
[27] H. Y Lee, H. G Kim, Thin solids films 229 (1993) 187.
[28] K.L. Siefering, G.L. Griffin, J. Electrochem. Soc. 137 (1990) 814.
[29] M.M. Chou, L. Chang, H. Y H. Huang, J.J. Wu, C.W. Chen, J. Cryst. Growth 308 (2007) 412.
[30] U. Backman, A. Auvinen, J.K. Jokiniemi, Surf. Coat. Technol. 192 (2005) 81.
[31] D.J. Won, C.H. Wang, H.K. Jang, D.J. Choi, Appl. Phys. A 73 (2001) 595.
[32] P. Babelon, A.S. Dequiedt, H. Mostefa, S. Bourgeois, P. Sibillot, M. Sacilotti, Thin Solid Films 322 (1997) 63.
[33] J. Dai, H. Liu, W. Fang, L. Wang, Y. Pu, Y. Chen, F. Jiang, J. Cryst. Growth 269 (2004) 356.
[34] B.P. Zhang, K. Wakatsukia, N.T. Binha, N. Usamic, Y. Segawa, J. Cryst. Growth 449 (2004) 12.
[35] F.D. Duminica, F. Maury, F. Senocq, Surf. Coat. Technol. 188–189 (2004) 225.
[36] D.J. Won, C.H. Wang, H.K. Jang, D.J. Choi, Appl. Phys. A 73 (2001) 595.
[37] Y. Kashiwaba, F. Katahira, K. Haga, T. Sekiguchi, H. Watanabe, J. Cryst. Growth 221 (2000) 431.
[38] J. Dai, H. Liu, W. Fang, L. Wang, Y. Pu, Y. Chen, F. Jiang, J. Cryst. Growth 283 (2005) 93.
[39] S. Muthkumar, H. Sheng, J. Zhong, Z. Zhang, N.W. Emanetoglu, Y. Lu, IEEE Trans. Nanotechnol. 2 (2003) 50.
[40] Y. Wang, S. Wang, S. Zhou, J. Xu, J. Ye, S. Gu, R. Zhang, Q. Ren, Appl. Surf. Sci. 253 (2006) 1745.
[41] X.W. Sun, H.S. Kwok, J. Appl. Phys. 86 (1999) 408.
[42] S.J. Henley, M.N.R. Ashfold, D. Cherns, Surf. Coat. Technol. 177 (2004) 271.
[43] R.D. Vispute, V. Talyanski, Z. Trajanovic, S. Choopun, M. Downes, R.P. Sharma, T. Venkatesan, Appl. Phys. Lett 70 (1997) 2735.
[44] M.P. Allen, D.J. Tildesley, Computer Simulation of Liquids, Oxford University Press, Oxford, 1989.
[45] R. Dreizler, E. Gross, Density Functional Theory, Plenum Press, New York, 1995.
[46] F. Claeyssens, C.L. Freeman, N.L. Allan, Y. Sun, M.N.R. Ashfold, J.H. Harding, J. Mater. Chem. 15 (2005) 139.
[47] C. Yang, Y. Yi, R. Li, Surf. Rev. Lett. 13 (2006) 27.
[48] D.C. Sayle, C. Richard, A. Catlow, N. Dulamita, M. Healy, S.A. Maicaneanu, B. Slater, G.W. Watson, Mol. Simulation 28 (2002) 683.
[49] A. Hasnaoui, O. Politano, J.M. Salazar, G. Aral, R.K. Kalia, A. Nakano, P. Vashishta, Surf. Sci. 579 (2005) 47.
[50] M. Taguchi, S. Hamaguchi, Thin Solid Films 515 (2007) 4879.
[51] http://www.cse.clrc.ac.uk/msi/software/DL_POLY.
[52] M. Born, K. Huang, Dynamical Theory of Crystal Lattices, Oxford Press, Oxford, 1968.
[53] G.V. Lewis, C.R.A. Catlow, J. Phys. C 18 (1985) 1149.
[54] F.A. Cotton, G. Wilkinson, Advanced Inorganic Chemistry, Wiley, New York, 1972.
[55] J.H. Rose, J.R. Smith, J. Ferrante, Phys. Rev. B 28 (1983) 1835.
[56] E.C. Behrman, R.K. Foehrweiser, J.R. Myers, B.R. French, M.E. Zandler, Phys. Rev. A 49 (1994) R1543.
[57] M. Matsui, M. Akaogi, Mol. Simulation 6 (1991) 239.
[58] H. Le Roux, L. Glasser, J. Mater. Chem. 7 (1997) 843.
[59] T.S. Bush, J.D. Gale, C.R.A. Catlow, P.D. Battle, J. Mater. Chem. 4 (1994) 831.
[60] J. Post, C. Burnham, Am. Mineral. 71 (1986) 142.
[61] R.G. Gordon, Y.S. Kim, J. Chem. Phys. 56 (1972) 3122.
[62] A.J. Kulkarni, M. Zhou, F.J. Ke, Nanotechnology 16 (2005) 2749.
[63] C.R.A. Catlow, Proc. R. Soc. London A 353 (1977) 533.
[64] R.W. Grimes, J. Am. Ceram. Soc 77 (1994) 378.
[65] E. Demiralp, T. Cagin, W.A. Goddard, Phys. Rev. Lett. 82 (1999) 1708.
[66] A. Takada, P. Richet, C.R.A. Catlow, G.D. Price, J. Non Cryst. Solid 345&346 (2004) 224.

[67] G. Malavasi, M.C. Menziani, A. Pedone, J. Non Cryst. Solids 352 (2006) 285.
[68] B. Vessal, J. Non Cryst. Solids 177 (1994) 103.
[69] W. Smith, G. N Greaves, M.J. Gillan, J. Chem. Phys. 103 (1995) 3091.
[70] M. Schaible, Crit. Rev. Solid State 24 (1999) 265.
[71] MINCRYST, ⟨http://database.iem.ac.ru/mincryst⟩.
[72] P.P. Ewald, Ann. Phys. 64 (1921) 253.
[73] M.V. Ramana, D.H. Phillips, J. Chem. Phys. 88 (1988) 2637.
[74] C.E. Housecroft, A.G. Sharpe, Inorganic Chemistry, Prentice Hall, Englewood Cliffs, 2001.
[75] A. Voter, F. Montalenti, T. Germann, Annu. Rev. Mater. Res. 32 (2002) 321.